



# Organic salt induced electrospinning gradient effect: Achievement of BiVO<sub>4</sub> nanotubes with promoted photocatalytic performance

Chade Lv<sup>a</sup>, Jingxue Sun<sup>a,b,\*</sup>, Gang Chen<sup>a,\*</sup>, Yansong Zhou<sup>a</sup>, Danying Li<sup>a</sup>, Zukun Wang<sup>a</sup>, Boran Zhao<sup>a</sup>

<sup>a</sup> MIIT Key Laboratory of Critical Materials Technology for New Energy Conversion and Storage, School of Chemistry and Chemical Engineering, Harbin Institute of Technology, Harbin, PR China

<sup>b</sup> School of Municipal and Environmental Engineering, State Key Laboratory of Urban Water Resource and Environment, Harbin Institute of Technology, Harbin 150001, PR China

## ARTICLE INFO

### Article history:

Received 14 November 2016  
Received in revised form 17 January 2017  
Accepted 17 February 2017  
Available online 20 February 2017

### Keywords:

Tubular nanostructure  
BiVO<sub>4</sub>  
Photocatalysis  
Electrospinning gradient effect  
Cr(VI) reduction

## ABSTRACT

Tubular nanostructure becomes the researchful focus in environmental purification because of its unique features, however, the hollow fibrous BiVO<sub>4</sub>, famous as an efficient photocatalyst for water purification and oxidation, has not been achieved yet. Here, we employ organic vanadium salt to fabricate BiVO<sub>4</sub> nanotubes by single-spinneret electrospinning without template. The organic salt can induce electrospinning gradient effect which plays a key role in the achievement of tubular nanostructure. Benefit from the unique structural properties of tubular nanostructure, BiVO<sub>4</sub> nanotubes possess hollow interior, leading to strong light harvesting ability and large surface areas. For photocatalytic reduction of Cr(VI), these contributions from tubular nanostructure could promote the photocatalytic performance relative to solid BiVO<sub>4</sub> nanofibers. This organic salt induced electrospinning gradient effect is not subject to the usage amount, ratio and kind of as-employed salt, endowing the electrospinning method with bright vista for the fabrication of other materials with tubular nanostructure.

© 2017 Elsevier B.V. All rights reserved.

## 1. Introduction

Photocatalysis has attracted intensive attention because it is sustainable and eco-friendly for tackling energy crisis and environmental issues [1,2]. As a low-cost and nontoxic photocatalyst, Titanium dioxide (TiO<sub>2</sub>) has been widely investigated in the past decades [3,4]. Nonetheless, owing to its large bandgap, only limited photon absorption under irradiation from sunlight could be utilized by TiO<sub>2</sub> [5,6]. Therefore, to solve this problem, many visible-light-driven photocatalysts are explored, for instance, BiOBr [7], C<sub>3</sub>N<sub>4</sub> [8,9], Ag<sub>3</sub>PO<sub>4</sub> [10,11] and Cd<sub>x</sub>Zn<sub>1-x</sub>S [12].

Monoclinic phase bismuth vanadate (BiVO<sub>4</sub>) has aroused intense interest as one of the most promising visible-light-driven photocatalysts due to the narrow bandgap and unique band structure [13–19]. Nevertheless, caused by its intrinsic drawbacks in separation and transfer of photoinduced charge carriers, the practical needs could not be met [20]. For the purpose of further

promoting the photocatalytic performance of BiVO<sub>4</sub>, nanostructuring is becoming a potentially overwhelming prospect for efficient pollution abatement and water oxidation [21–23].

An emerging approach is the reasonable design and fabrication of tubular nanostructure possessing low-dimensional and hollow properties, which offer fascinating application in electrochemistry [24] and photocatalysis [25]. Currently, electrospinning technique has been rapidly developed with unsubstitutability for facile synthesis of a large proportion of inorganic tubular nanomaterials [26–28]. However, to the best of our knowledge, there is no attempts on the fabrication of BiVO<sub>4</sub> nanotubes by electrospinning.

To electrospin nanotubes, Xia et al. proposed a coaxial electrospinning method by employing a coaxial spinneret [29]. Lou et al. fabricated M<sub>x</sub>Co<sub>3-x</sub>S<sub>4</sub> (M = Ni, Mn, Zn) nanotubes using electrospun fibrous PAN template [30]. For getting rid of the complexity of abovementioned method, Niu et al. have proposed a gradient electrospinning and controlled pyrolysis methodology [31]. The key point of this method is gradient distribution of polymer during the electrospinning process. In addition, the dominant component of tube walls is carbon derived from as-employed polymer. As the spinnable sols contain salt and polymer, it is speculated that fabrication of nanotubes without carbon phase components could be achieved by gradient distribution of salt. However, partial inor-

\* Corresponding authors at: MIIT Key Laboratory of Critical Materials Technology for New Energy Conversion and Storage, School of Chemistry and Chemical Engineering, Harbin Institute of Technology, Harbin, PR China.

E-mail addresses: [jxsun@hit.edu.cn](mailto:jxsun@hit.edu.cn) (J. Sun), [gchen@hit.edu.cn](mailto:gchen@hit.edu.cn) (G. Chen).

ganic salts lack of compatibility with the organic solvents used for electrospinning, therefore the ion migration mobility is not strong enough to realize the salt gradient. Inspired by this idea, to induce salt gradient electrospinning, organic salt could be utilized as reactant due to its good solubleness in organic solvents applied for electrospinning.

Herein, tubular BiVO<sub>4</sub> was achieved via electrospinning with an ordinary spinneret while bismuth nitrate pentahydrate (Bi(NO<sub>3</sub>)<sub>3</sub>·5H<sub>2</sub>O) and organic vanadium(IV)oxy acetylacetone (VO(acac)<sub>2</sub>) served as bismuth and vanadium sources in the precursor sols, respectively. And the BiVO<sub>4</sub> nanotubes with hollow structure were eventually obtained after subsequent calcination. In contrast, BiVO<sub>4</sub> nanofibers with solid interior were fabricated by using inorganic NH<sub>4</sub>VO<sub>3</sub>, instead, which is the only variable in the synthesis process. The employment of organic salt can induce electrospinning gradient, which determines the construction of tubular structure of BiVO<sub>4</sub>. Even though the change in salt amount, salt ratio and salt species, the electrospinning gradient effect induced by organic salt still works for fabricating tubular structure. Attributed to the unique properties of tubular nanostructure, large surface area, mesoporosity and enhanced light harvesting are achieved in BiVO<sub>4</sub> nanotubes. These favorable features endow BiVO<sub>4</sub> nanotubes with exceptional photocatalytic properties when evaluated as photocatalysts for reduction of Cr(VI).

## 2. Experimental

All reagents were received from Aladdin Chemical Co., Ltd., and used without further purification.

### 2.1. Electrospinning BiVO<sub>4</sub> nanotubes and nanofibers

In a typical synthesis, 0.485 g (1.0 mmol) of Bi(NO<sub>3</sub>)<sub>3</sub>·5H<sub>2</sub>O was dissolved in 8 mL of DMF (N,N-Dimethylformamide) with magnetic stirring at room temperature, and then 6 mL acetic acid was added into the mixture. After the Bi(NO<sub>3</sub>)<sub>3</sub>·5H<sub>2</sub>O dissolved, 0.265 g (1.0 mmol) VO(acac)<sub>2</sub> (Vanadium(IV)oxy Acetylacetone) was added slowly into above Bi(NO<sub>3</sub>)<sub>3</sub> solution. Then, 8 mL absolute ethanol was added. Afterward, 2.0 g PVP (*Mw* ≈ 1300000) was added slowly into above solution. The precursor sols were eventually obtained after continuous stirring overnight. All the precursor sols were transferred into a syringe attached to a needle with an inner diameter of 0.901 mm. The positive voltage applied to the tip was 16 kV and the distance between the needle tip and the collector was 14 cm. The feeding rate was controlled as 0.4 mL h<sup>-1</sup> and the humidity level is maintained around 25% RH. The as-spun fibers were calcinated at 500 °C in air for 30 min at a heating rate of 2 °C min<sup>-1</sup> (denoted as BVNTs). BiVO<sub>4</sub> nanofibers were fabricated by employing NH<sub>4</sub>VO<sub>3</sub> as vanadium source. Bi<sub>4</sub>V<sub>2</sub>O<sub>11</sub> nanotubes are synthesized by using 2 mmol Bi(NO<sub>3</sub>)<sub>3</sub> as Bi source and 1 mmol VO(acac)<sub>2</sub> as V source, respectively. Bi<sub>4</sub>V<sub>2</sub>O<sub>11</sub> nanofibers were prepared with 2 mmol Bi(NO<sub>3</sub>)<sub>3</sub> and 1 mmol NH<sub>4</sub>VO<sub>3</sub>. Ni<sub>3</sub>V<sub>2</sub>O<sub>8</sub> nanotubes were fabricated by employing 1.5 mmol Ni(NO<sub>3</sub>)<sub>2</sub> and 1 mmol VO(acac)<sub>2</sub>. The calcination process was the same as that of BVNTs.

### 2.2. Characterizations

The structure of the obtained samples was confirmed by X-ray diffraction (XRD) on Rigaku D/max-2000 diffractometer with Cu K $\alpha$  radiation ( $\lambda = 0.15406$  nm). Diffraction patterns were collected from 10° to 90° at a speed of 4° min<sup>-1</sup> with a scan width of 0.02°. The morphology of the samples were observed by a HELIOS NanoLab 600i field emission scanning electron micro-scope (FE-SEM). The operating voltage was set to 20 kV and the samples were prepared by dropping the pre-ultrasonic-dispersed (10 min) ethanol turbid

liquid onto the chip of silicon. Transmission electron microscopy (TEM) and high-resolution TEM (HRTEM) of the BiVO<sub>4</sub> nanotubes were carried out on FEI Tecnai G2 F30 S-Twin operating at 300 kV. X-ray photoelectron spectroscopy (XPS) was accomplished using a Thermo Scientific ESCALAB 250Xi X-ray photoelectron spectrometer with a pass energy of 20.00 eV and an Al K $\alpha$  excitation source (1486.6 eV). Infrared (IR) analysis of the samples was carried out on a FT-IR spectrometer (Shimadzu) in the form of KBr pellets. UV-vis diffuse reflectance spectra were acquired by a spectrophotometer (TU-1901) and BaSO<sub>4</sub> was used as the reflectance standard.

### 2.3. Photocatalytic measurements

The reduction of Cr(VI) was irradiated with the visible light source by using a 300 W Xe lamp (Trusttech PLS-SXE 300, Beijing) with a cutoff filter ( $\lambda \geq 400$  nm) in the presence of citric acid. In a typical process, 0.05 g of the as-prepared sample as photocatalyst was added into 100 mL of Cr(VI) solution (10 mg L<sup>-1</sup>, which was based on Cr in a dilute K<sub>2</sub>Cr<sub>2</sub>O<sub>7</sub> solution). After the photocatalyst was dispersed in the solution with an ultrasonic bath for 5 min, the solution was stirred for 55 min in the dark to reach adsorption equilibrium. Before being exposed to visible-light irradiation, 0.05 g citric acid was added into the solution. The photocatalyst was removed by centrifugation at given time intervals, and the Cr(VI) concentration was determined at 540 nm by the diphenylcarbazide (DPC) method using the UV-vis spectroscopy [32,33].

## 3. Results and discussion

### 3.1. Structure and morphology analysis of BVNTs and BVNPs

In order to fabricate BiVO<sub>4</sub> nanotubes, VO(acac)<sub>2</sub>, a soluble organic vanadium source, served as vanadium source. The as-spun fibers of BiVO<sub>4</sub> nanotubes (denoted as BVNTs) are uniform with about 200 nm in diameter (Fig. 1a, b). After the heat treatment of as-spun fibers at 500 °C, the as-calcined BiVO<sub>4</sub> exhibits the morphology of porous nanotubes with *ca.* 200 nm in diameter (Fig. 1c, d) and the cross-section of the nanotubes is magnified in the insert image of Fig. 1d. In addition, monoclinic BiVO<sub>4</sub> structure (JCPDS: No. 14-0688) is confirmed as displayed in the XRD pattern (Fig. 2).

As observed in TEM images (Fig. 3a, b), the as-fabricated samples are mesoporous (20 nm in pore size) and uniform in diameter (about 200 nm), which is in accordance with SEM images shown above. The primary particle size is approximately 40 nm. Moreover, as the decomposition of PVP and other ingredients occurs during the heat treatment process [34,35], the disappearance of shrinkage on BVNTs implies the formation of hollow structure in BVNTs. The HAADF images shown in Fig. 3c, d further confirm the tubular structure of BVNTs. The line scan of BVNTs demonstrates that the Bi, V and O are homogeneously distributed (Fig. 3e). Fig. 3f reveals that the nanoparticles which constituted the BVNTs are well defined with the (121) plane of monoclinic BiVO<sub>4</sub>, which is consistent with the XRD result. Selected area electron diffraction (SAED) pattern (the insert image of Fig. 3f) indicates the poly-crystalline nature of the BVNTs. From above, by utilizing organic VO(acac)<sub>2</sub>, we successfully fabricate BiVO<sub>4</sub> mesoporous nanotubes which are constructed by interconnected monoclinic BiVO<sub>4</sub> nanoparticles.

For BiVO<sub>4</sub> nanofibers (denoted as BVNPs), the electrospinning process and subsequent calcination procedure are the same as that of the BVNTs, while organic vanadium source is replaced by inorganic NH<sub>4</sub>VO<sub>3</sub>. The as-spun fibers exhibit uniform morphology in diameter which is as thin as that of BVNTs (Fig. 4a, b). After the heat treatment of as-spun fibers, we obtain BiVO<sub>4</sub> nanofibers of diameter around 100 nm constructed from attached nanoparticles (Fig. 4c, d). The obvious decrease in diameter of as-calcined nanofibers

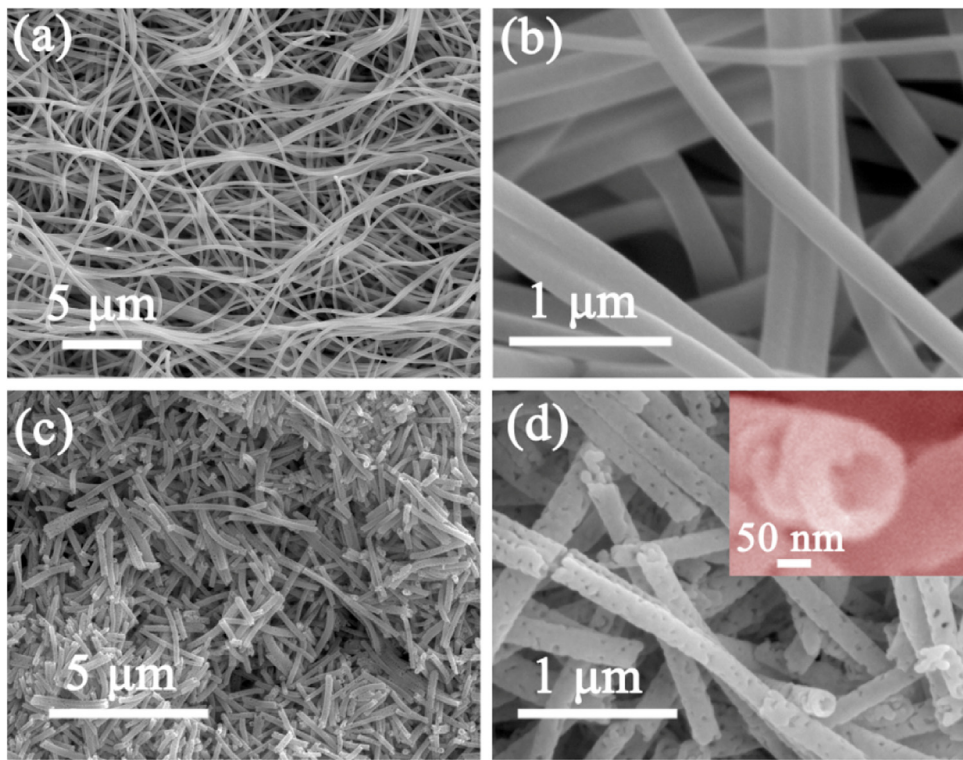


**Fig. 1.** SEM images of BVNTs: before (a, b) and after (c, d) calcination.

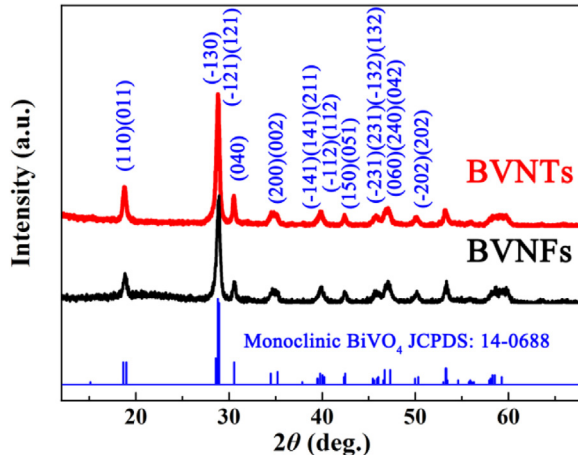


**Fig. 2.** XRD pattern of BVNTs and BVNPs.

manifests the presence of shrinkage, which is comparatively different from the evolution process of BVNTs. XRD result in Fig. 2 reveals the as-fabricated nanofibers are BiVO<sub>4</sub> monoclinic structure. Above all, employing inorganic NH<sub>4</sub>VO<sub>3</sub> as vanadate source determined the formation of nanofibers with solid interior, while the phase structure of monoclinic BiVO<sub>4</sub> could be obtained without being affected. However, because the primary particle size is approximately 30 nm, which is slightly smaller than that of BVNTs, the crystallinity of BVNPs is not as good as that of BVNTs.

### 3.2. Formation mechanism analysis of tubular structure

Considering that calcination process of BVNTs is consistent with that of BVNPs, the formation tubular structure could be attributed to the difference in surface chemical ingredient of as-spun fibers.

Therefore, the distribution of surface element in as-spun fibers of BVNTs and BVNPs based on the Bi 4f and V 2p XPS spectra are summarized in Fig. 5a, b [36]. By comparing the peak intensity between Bi 4f and V 2p, it could be confirmed that the atomic concentration ratio between Bi and V at the surface of the as-spun fibers in BVNTs is decreased. The relatively slight enhancement in vanadium atomic concentration at the surface could be due to the stronger migration ability of organic vanadium salt in as-employed solvents. Moreover, as shown in FT-IR spectra (Fig. S1), the C=O band around 1630 cm<sup>-1</sup> of BVNTs is enhanced which could be stemmed from acetylacetone in VO(acac)<sub>2</sub>. Besides, two bands around 877 and the 1042 cm<sup>-1</sup> stand out which are assigned to the asymmetric stretching of the V—O—V bond and V=O stretching vibration in VO(acac)<sub>2</sub>, respectively [37]. Therefore, the FT-IR spectra of the as-spun fibers could further affirm above results. The distinction in surface chemical ingredient of as-spun fibers could certify the presence of salt gradient induced by organic salt.

Based on abovementioned observations, an organic salt induced electrospinning gradient effect is proposed as below in order to illustrate the formation mechanism of BVNTs (Fig. 6). At the electrospinning stage, Bi(NO<sub>3</sub>)<sub>3</sub>, VO(acac)<sub>2</sub> and PVP are distributed uniformly in the spinnable sols. Once the electrostatic field force overcame the surface tension, a charged jet flow is spewed out from the needle tip. During that process, the solvents would evaporate at a fairly fast rate. Generally, solvent volatilization at the surface is faster than that at centred solvent part, leading to the decrease of solvents content at the surface compared with that of the internal region. Therefore, a concentration gradient of solvent would generate along the radial direction of the jet flow, pushing the system into an unstable phase state eventually. The driving force offered by above concentration gradient worked on the salt ions simultaneously [38,39]. For BVNTs, as-employed Bi(NO<sub>3</sub>)<sub>3</sub> and VO(acac)<sub>2</sub> possess a certain degree of solubility in the solvent, hence salt ions could migrate to the shell region of nanofiber in company with the solvent motion. As a result, a salt gradient arises as illustrated in

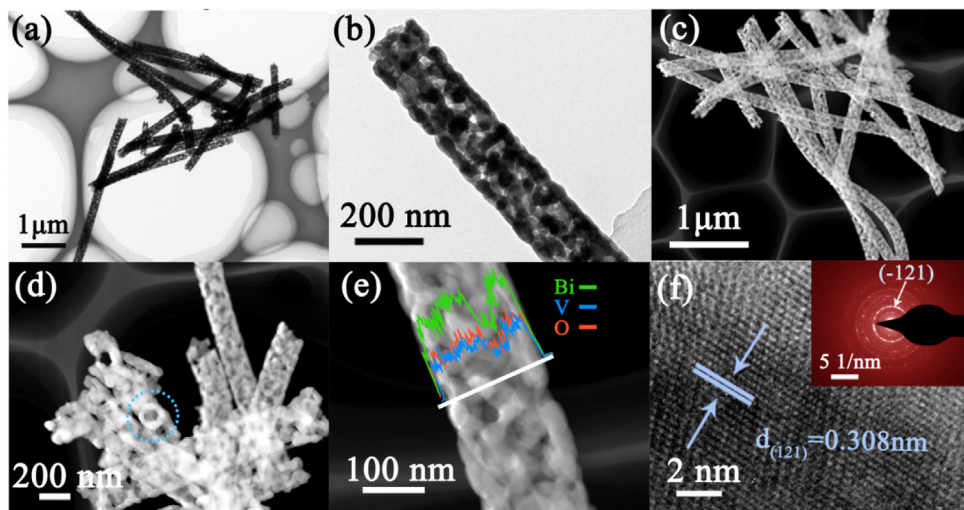


**Fig. 3.** TEM characterization of BVNTs: (a, b) TEM images, (c, d) HAADF images, (e) line scan profile, (f) HRTEM image and the insert image is corresponding SAED pattern.

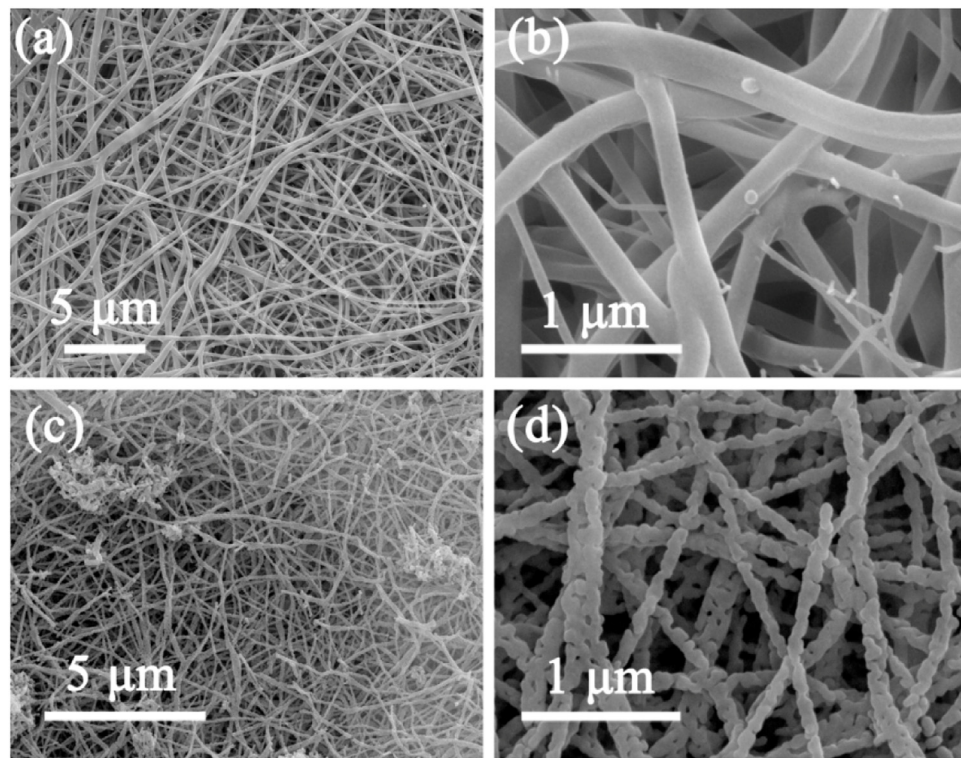


**Fig. 4.** SEM images of BVNFs: before (a, b) and after (c, d) calcination.

**Fig. 6.** When the solvents volatilize completely, the jet flow develops into as-spun fibers, in which the  $\text{Bi}(\text{NO}_3)_3$ ,  $\text{VO}(\text{acac})_2$  and a small portion of PVP constitute the shell together. During the calcination process,  $\text{Bi}(\text{NO}_3)_3$  and  $\text{VO}(\text{acac})_2$  decompose, bringing about to the subsequent crystal growth of  $\text{BiVO}_4$ . As the outer region consists of  $\text{Bi}(\text{NO}_3)_3$  and  $\text{VO}(\text{acac})_2$ , the  $\text{BiVO}_4$  shell form gradually. In addition, ascribed to “surface locking” effect of as-generated  $\text{BiVO}_4$  crust, further inward shrinkage and the diameter of the fibers are “frozen”, which is shown in SEM images (Fig. 1) [40]. At the same time, as a consequence of the burning out of PVP, the nanotubes are obtained possessing hollow interior and mesopores. The “surface locking” could protect the  $\text{BiVO}_4$  nanoparticles from aggregation, reserving the mesopores on the surface of BVNTs. For BVNFs, the

preliminary solvents volatilization process of BVNFs is the same as that of BVNTs because the selection of  $\text{NH}_4\text{VO}_3$  is the only variate. However, due to the intrinsic difference in solubleness of  $\text{Bi}(\text{NO}_3)_3$  and  $\text{NH}_4\text{VO}_3$  (the solubility of  $\text{NH}_4\text{VO}_3$  in ethanol and DMF is poor), even though solvents gradient still appear, the diffusion rate of  $\text{Bi}(\text{NO}_3)_3$  is much higher than that of  $\text{NH}_4\text{VO}_3$ . Thus, the  $\text{NH}_4\text{VO}_3$  is distributed homogeneously in the as-spun fibers, while Bi migrates to the shell layer. When the as-spun fibers are annealed at high temperature, outer  $\text{Bi}(\text{NO}_3)_3$  diffuses inward toward the internal  $\text{NH}_4\text{VO}_3$  and  $\text{BiVO}_4$  particles are generated, which is proved by the shrinkage phenomenon of BVNFs. Besides, attributed to the shrinkage and owtwald ripening process, the  $\text{BiVO}_4$  nanoparticles attach with each other, forming the solid BVNFs.

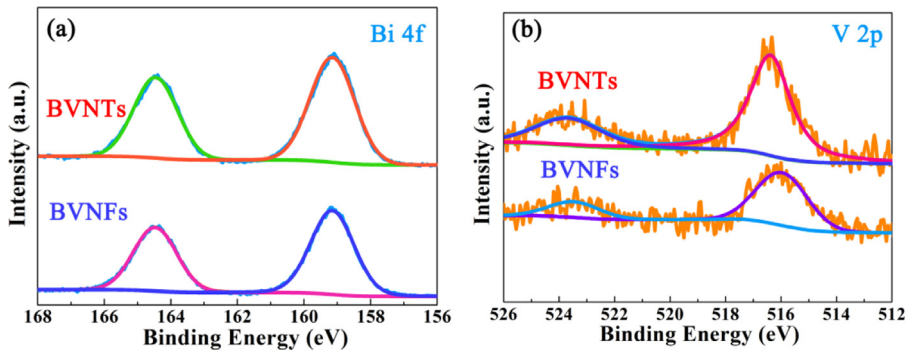


**Fig. 5.** XPS spectra of as-spun fibers: (a) Bi4f, (b) V2p.

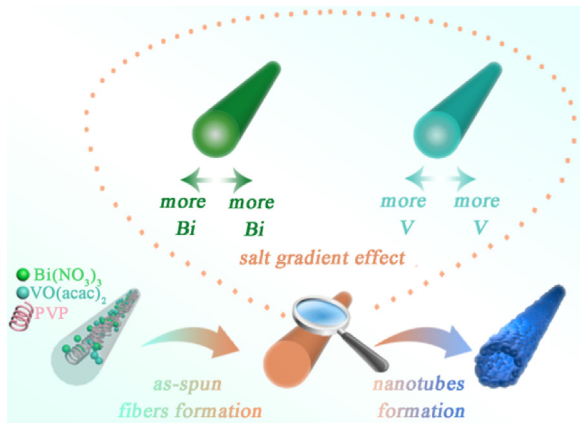


**Fig. 6.** Formation mechanism of tubular BiVO<sub>4</sub>.

### 3.3. Feasibility analysis of proposed formation mechanism

Ulteriorly, to rule out the influence of salt addition amount, which could affect the formation process of as-calcinated product, BiVO<sub>4</sub> nanotubes are also fabricated with more Bi(NO<sub>3</sub>)<sub>3</sub> and organic VO(acac)<sub>2</sub>. As observed in Fig. 7a and b, even though 2 mmol Bi(NO<sub>3</sub>)<sub>3</sub> and VO(acac)<sub>2</sub> or 3 mmol Bi(NO<sub>3</sub>)<sub>3</sub> and VO(acac)<sub>2</sub> are added, the calcination products are nanotubes with hollow interior, indicating the organic salt induced electrospinning gradient effect is not limited by salt amount.

For the purpose of further confirming the mechanism of organic salt induced electrospinning gradient effect, Bi<sub>4</sub>V<sub>2</sub>O<sub>11</sub> and Ni<sub>3</sub>V<sub>2</sub>O<sub>8</sub> nanotubes are also fabricated by employing organic VO(acac)<sub>2</sub> as vanadium source. As shown in Fig. 7c, porous Bi<sub>4</sub>V<sub>2</sub>O<sub>11</sub> nanotubes are obtained with hollow interior (XRD pattern is shown in Fig. S2), which are similar with the morphology of BVNTs. However, replacing the organic VO(acac)<sub>2</sub> with inorganic NH<sub>4</sub>VO<sub>3</sub> only contributes to the formation of Bi<sub>4</sub>V<sub>2</sub>O<sub>11</sub> nanofibers (Fig. S3), which is consistent with that of BVNPs. The successful preparation of Bi<sub>4</sub>V<sub>2</sub>O<sub>11</sub>

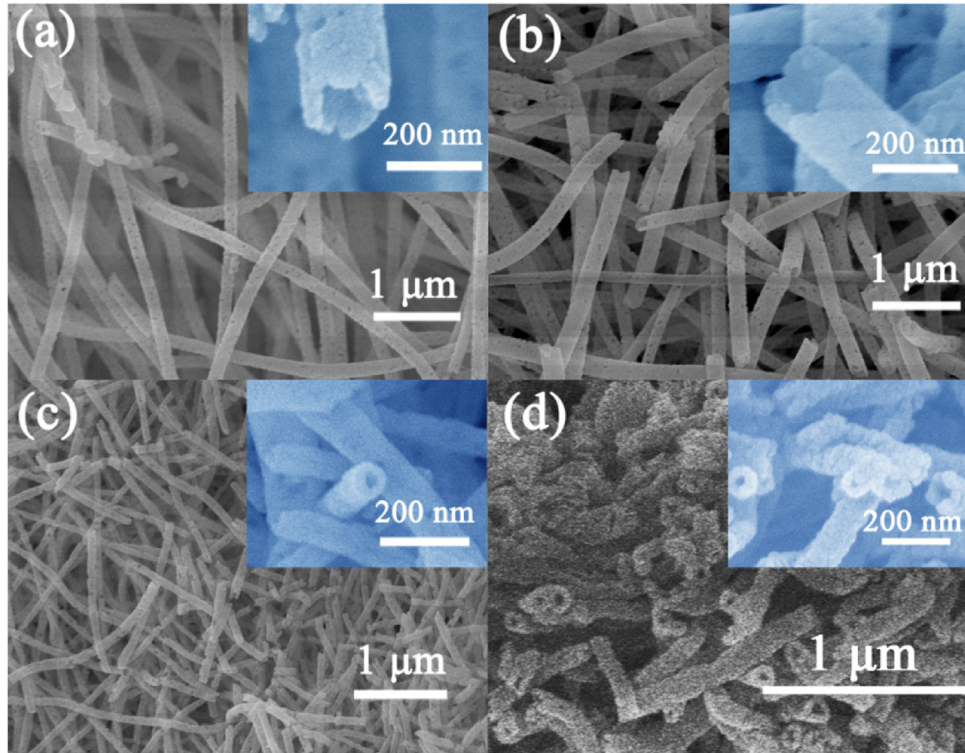


**Fig. 7.** SEM images of BiVO<sub>4</sub>, Bi<sub>4</sub>V<sub>2</sub>O<sub>11</sub> and Ni<sub>3</sub>V<sub>2</sub>O<sub>8</sub> nanotubes: (a) BiVO<sub>4</sub> nanotubes with 2 mmol Bi(NO<sub>3</sub>)<sub>3</sub> and VO(acac)<sub>2</sub>, (b) BiVO<sub>4</sub> nanotubes with 3 mmol Bi(NO<sub>3</sub>)<sub>3</sub> and VO(acac)<sub>2</sub>, (c) Bi<sub>4</sub>V<sub>2</sub>O<sub>11</sub> nanotubes, (d) Ni<sub>3</sub>V<sub>2</sub>O<sub>8</sub> nanotubes.

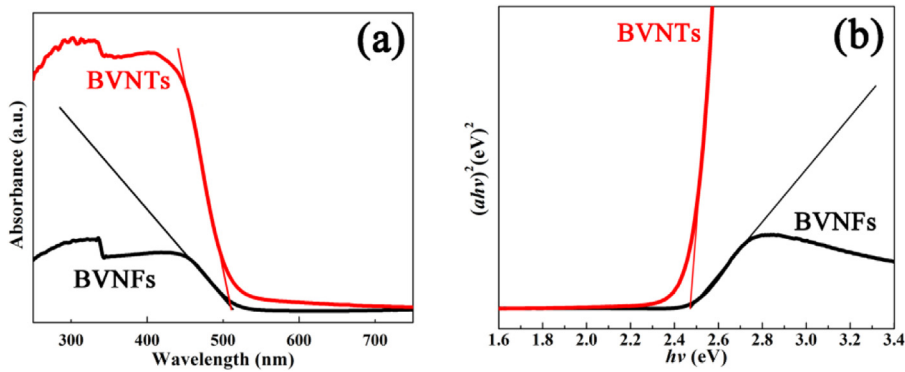


**Fig. 8.** Optical absorption properties of the samples: (a) UV-vis diffuse reflectance spectra, (b) the plots of  $(\alpha h v)^{n/2}$  vs  $h v$  ( $n=4$ ).

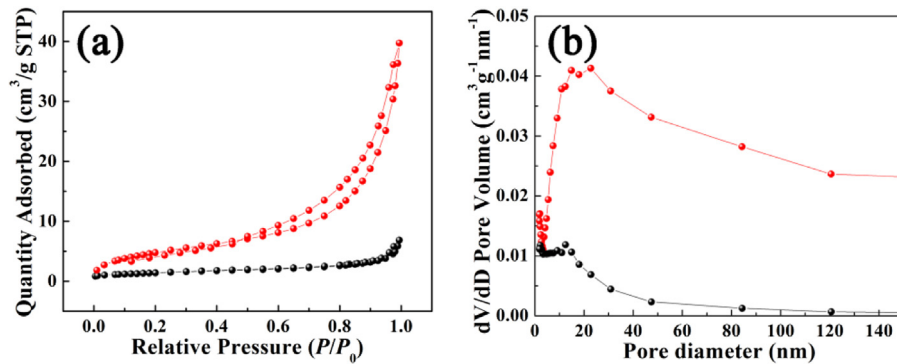


**Fig. 9.** (a) N<sub>2</sub> adsorption–desorption isotherms of BVNTs and BVNPs, (b) BJH desorption pore size distribution plots.

nanotubes demonstrates that the Bi/V ratio is not the determinant factor in realizing the salt gradient effect, nevertheless, the organic salt plays a decisive role. As shown in Fig. 7d, we also obtain the Ni<sub>3</sub>V<sub>2</sub>O<sub>8</sub> nanotubes by using Ni(NO<sub>3</sub>)<sub>2</sub> and VO(acac)<sub>2</sub>, and the XRD pattern is displayed in Fig. S4. Similarly, only solid Ni<sub>3</sub>V<sub>2</sub>O<sub>8</sub> nanofibers are obtained after replacing the organic VO(acac)<sub>2</sub> with inorganic NH<sub>4</sub>VO<sub>3</sub> (Fig. S5). Despite of changing the as-employed inorganic salt, the nanotubes are also achieved using VO(acac)<sub>2</sub>, implying that suitable adoption of organic salt achieved the electro-spinning gradient effect, which could be applied to fabricate other tubular nanomaterials. Accordingly, based on above experimental results, we draw a conclusion that the rational employment of organic salt plays a key role on the achievement of electrospinning gradient effect, which realized the successful construction of BiVO<sub>4</sub> nanotubes.

#### 3.4. UV-vis DRS and BET

With the aim of evaluating the impact of nanotubes structure on the optical properties (such as band gap) of BiVO<sub>4</sub>, which could be a key factor for photocatalysis, the UV-vis diffusion reflection spectra are performed. As shown in Fig. 8a, the BVNTs and BVNPs exhibit visible light absorbance and the absorbance edges locate at around 530 nm. The as-calculated bandgap values of BVNTs and BVNPs are around 2.45 eV (Fig. 8b). The inconspicuous change of band gap indicates that the construction of tube-like nanostructure on BiVO<sub>4</sub> had negligible impact on the band structure. Nevertheless, the optical absorption of BVNPs is reduced dramatically relative to BVNTs. The outstanding light-harvesting ability of BVNTs could be attributed to the hollow interior structure of nanotube, which endow the BVNTs with high density of internal “reflection mirror” for repeated light utilization [41]. Moreover, the detailed values of CB and VB are calculated by combining Mott-Schottky measure-

ment and UV-vis DRS spectra. As shown in Mott-Schottky plots (Fig. S6), the CB value of BVNTs is -0.44 eV (vs. Ag/AgCl). As a result, the VB value is 2.01 eV (vs. Ag/AgCl) according to the bandgap value calculated from UV-vis DRS spectra.

Besides the promoted light-harvesting caused from constructing tubular nanostructure on BiVO<sub>4</sub>, mesopores and hollow interior of nanotubes could also contribute to the enhancement of specific areas. As exhibited in Fig. 9a, the BET surface area of BVNTs presents a relatively high value, about 17.96 m<sup>2</sup> g<sup>-1</sup>, which is 3 times higher than that of BVNPs (5.04 m<sup>2</sup> g<sup>-1</sup>). Fig. 9b contrasts the pore size-distribution curves between BVNTs and BVNPs. 22 nm is the dominated size for BVNTs, indicating the nanotubes possess mesoporous structure, which is well matched with TEM images shown above. As compared with BVNTs, the BVNPs do not exhibit obvious porous property due to their solid structure.

#### 3.5. Photocatalytic reduction of Cr(VI) measurement and mechanism analysis

These BVNTs possess above superiority as a result of constructing tubular nanostructure on BiVO<sub>4</sub>, therefore, they could find potential uses in photocatalysis. Here, we evaluate their promising application as photocatalyst for photocatalytic reduction of Cr(VI). The photocatalytic reduction of Cr(VI) among BVNTs and BVNPs under visible-light irradiation is investigated as shown in Fig. 10a. Without the addition of catalysts, Cr(VI) could not be reduced under the same condition. However, the Cr(VI) could be reduced after the introduction of catalysts. In a sharp contrast, the BVNTs exhibit better photocatalytic performance with 95.3% of Cr(VI) degraded after irradiation for 80 min. Meanwhile, BVNPs display much lower activity, which only reaches 50% of Cr(VI). As shown in Fig. 10b, the BVNTs exhibits a good cycling performance (Fig. 10b). Furthermore, as determined by XPS analysis of the BVNTs samples after

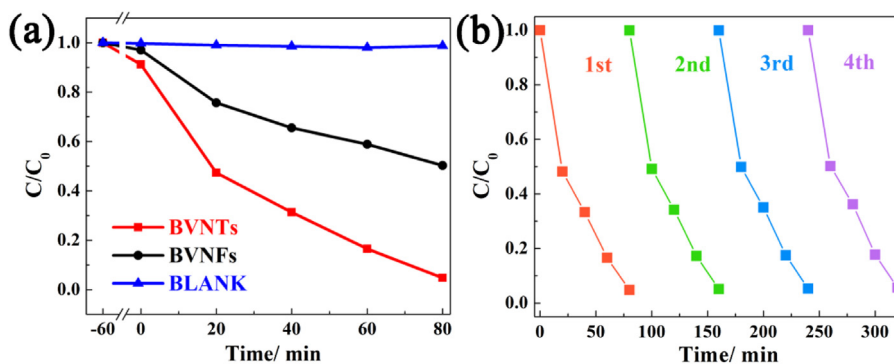


**Fig. 10.** (a) Dynamic curves of Cr(VI) solution over as-calciated samples under visible light, (b) cycle photocatalytic reduction of Cr(VI) over BVNTs.

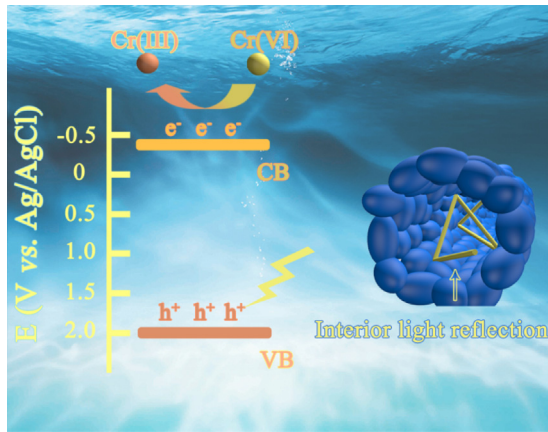


**Fig. 11.** Photocatalytic mechanism of BVNTs.

the photocatalysis experiment (Fig. S7), no Cr(III) can be found on the surface of BVNTs, indicating the reduced Cr(III) ions exist in the solution. The clear surface of BVNTs after the photocatalysis experiment could guarantee the excellent cycling performance of BVNTs.

The reasons for promoted photocatalytic activity could be illustrated in Fig. 11 and summarized as follows: (1) The interior hollow structure of BVNTs offers reflection surface, where light could be reflected repeatedly, leading to more effective light-harvesting for photocatalysis; (2) Owing to the hollow interior and mesoporous structure, BVNTs possess higher surface area than BVNPs, which could furnish more active sites for photocatalysis reaction, determining the better photocatalytic activity towards reduction of Cr(VI).

Moreover, the promoted photocatalytic activity of BVNTs might also originate from the slight enhancement in crystallinity. The crystallinity can also be influenced by the calcination temperature, which might be another factor to enhance the photocatalytic performance. To verify abovementioned speculation, the as-spun fibers are calcinated at 550 °C and 600 °C (denoted as BVNTs-550 and BVNTs-600, respectively). As displayed in Fig. S8, the crystallinity of the samples becomes better as the calcination temperature increases. When evaluated as catalysts for reduction of Cr(VI), the BVNTs obtained at 500 °C delivers the best photocatalytic activity among the samples (Fig. S9). Even though the BVNTs calcinated at 550 and 600 °C possess better crystallinity in relative to BVNTs obtained at 500 °C, the photocatalytic performance can not reach the same level as that obtained at 500 °C. The enhanced crystallinity could be stemmed from the increased primary particle size of the samples, which might result in the decrease of surface area, leading to the decline of catalytic activity [42]. Therefore, the

tubular structure induced enhanced BET surface area and interior light reflection play the determinant role in promoting the photocatalytic properties. Meanwhile, the slightly enhanced crystallinity of BVNTs can also contribute the enhancement in photocatalytic performance.

#### 4. Conclusions

In summary, we have fabricated mesoporous BiVO<sub>4</sub> nanotubes (BVNTs) via a single spinneret electrospinning method with subsequent calcination. The employment of organic salt is the key factor to achieve electrospinning gradient effect, which realizes the successful construction of tubular nanostructure. The appearance of hollow interior and mesopores endows the BiVO<sub>4</sub> nanotubes with stronger light-harvesting ability and much higher surface area. The BVNTs exhibit promoted photocatalytic activity towards the reduction of Cr(VI) relative to BVNPs. This work could offer new inspiration for the rational utilization of electrospinning technique to fabricate more one-dimensional tubular nanomaterials for nanostructure-related application.

#### Acknowledgements

This work was financially supported by the National Nature Science Foundation of China (21501035, 21471040) and China Postdoctoral Science Foundation funded project (2015M570298 and 2016T90301). We acknowledge for the support by HIT Environment and Ecology Innovation Special Funds (No. HSCJ201616).

#### Appendix A. Supplementary data

Supplementary data associated with this article can be found, in the online version, at <http://dx.doi.org/10.1016/j.apcatb.2017.02.058>.

#### References

- [1] Y.Q. Qu, X.F. Duan, Chem. Soc. Rev. 42 (2013) 2580.
- [2] H.L. Wang, L.S. Zhang, Z.G. Chen, J.Q. Hu, S.J. Li, Z.H. Wang, J.S. Liu, X.C. Wang, Chem. Soc. Rev. Chem. Soc. Rev. 43 (2014) 5234–5244.
- [3] J. Schneider, M. Matsuoka, M. Takeuchi, J.L. Zhang, Y. Horiuchi, M. Anpo, D.W. Bahnemann, Chem. Rev. 114 (2014) 9919–9986.
- [4] X.J. Lang, W.H. Ma, C.C. Chen, H.W. Ji, J.C. Zhao, Acc. Chem. Res. 47 (2014) 355–363.
- [5] R. Inde, M. Liu, D. Atarashi, E. Sakaia, M. Miyauchi, J. Mater. Chem. A 4 (2016) 1784–1791.
- [6] X.B. Chen, L. Liu, F.Q. Huang, Chem. Soc. Rev. 44 (2015) 1861–1885.
- [7] H. Li, J. Shang, Z.H. Ai, L.Z. Zhang, J. Am. Chem. Soc. 137 (2015) 6393–6399.
- [8] W.-J. Ong, L.-L. Tan, Y.H. Ng, S.-T. Yong, S.-P. Chai, Chem. Rev. 116 (2016) 7159–7329.
- [9] F. He, G. Chen, J.W. Miao, Z.X. Wang, D.M. Su, S. Liu, W.Z. Cai, L.P. Zhang, S.E. Hao, B. Liu, ACS Energy Lett. 1 (2016) 969–975.

- [10] Z.G. Yi, J.H. Ye, N. Kikugawa, T. Kako, S.X. Ouyang, H. Stuart-Williams, H. Yang, J.Y. Cao, W.J. Luo, Z.S. Li, Y. Liu, R.L. Withers, *Nat. Mater.* 9 (2010) 559–564.
- [11] P.Y. Dong, Y.H. Wang, B.C. Cao, S.Y. Xin, L.N. Guo, J. Zhang, F.H. Li, *Appl. Catal. B: Environ.* 132–133 (2013) 45–53.
- [12] M.C. Liu, Y.B. Chen, J.Z. Su, J.W. Shi, X.X. Wang, L.J. Guo, *Nat. Energy* 1 (2016) 16151.
- [13] Y. Park, K.J. McDonald, K.S. Choi, *Chem. Soc. Rev.* 42 (2013) 2321–2337.
- [14] S.W. Liu, K. Yin, W.S. Ren, B. Cheng, J.G. Yu, *J. Mater. Chem.* 22 (2012) 17759–17767.
- [15] M.L. Guan, D.K. Ma, S.W. Hu, Y.J. Chen, S.M. Huang, *Inorg. Chem.* 50 (2011) 800–805.
- [16] D.K. Ma, M.L. Guan, S.S. Liu, Y.Q. Zhang, C.W. Zhang, Y.X. He, S.M. Huang, *Dalton Trans.* 41 (2012) 5581–5586.
- [17] P. Cai, S.M. Zhou, D.K. Ma, S.N. Liu, W. Chen, S.M. Huang, *Nano-Micro Lett.* 7 (2015) 183–193.
- [18] L.N. Wang, D.X. Han, S. Ni, W.G. Ma, W. Wang, L. Niu, *Chem. Sci.* 6 (2015) 6632–6638.
- [19] H.Y. Li, Y.J. Sun, B. Cai, S.Y. Gan, D.X. Han, L. Niu, T.S. Wu, *Appl. Catal. B: Environ.* 170–171 (2015) 206–214.
- [20] N. Tian, H.W. Huang, Y. He, Y.X. Guo, T.R. Zhang, Y.H. Zhang, *Dalton Trans.* 44 (2015) 4297–4307.
- [21] G.C. Xi, J.H. Ye, *Chem. Commun.* 46 (2010) 1893–1895.
- [22] K.M. Ji, H.X. Dai, J.G. Deng, H.J. Zang, H. Arandiyan, S.H. Xie, H.G. Yang, *Appl. Catal. B: Environ.* 168–169 (2015) 274–282.
- [23] S.M. Sun, W.Z. Wang, D.Z. Li, L. Zhang, D. Jiang, *ACS Catal.* 4 (2014) 3498–3503.
- [24] S.M. Dong, X. Chen, L. Gu, X.H. Zhou, L.F. Li, Z.H. Liu, P.X. Han, H.X. Xu, J.H. Yao, H.B. Wang, X.Y. Zhang, C.Q. Shang, G.L. Cui, L.Q. Chen, *Energy Environ. Sci.* 4 (2011) 3502–3508.
- [25] F.X. Xiao, J.W. Miao, H.B. Tao, S.F. Hung, H.Y. Wang, H.B. Yang, J.Z. Chen, R. Chen, B. Liu, *Small* 11 (2015) 2115–2131.
- [26] T. Krishnamoorthy, V. Thavasi, G.M. Subodh, S. Ramakrishna, *Energy Environ. Sci.* 4 (2011) 2807–2812.
- [27] S.J. Peng, G.R. Jin, L.L. Li, K. Li, M. Srinivasan, S. Ramakrishna, J. Chen, *Chem. Soc. Rev.* 45 (2016) 1225–1241.
- [28] D.M. Yu, C.G. Chen, S.H. Xie, Y.Y. Liu, K. Park, X.Y. Zhou, Q.F. Zhang, J.Y. Li, G.Z. Cao, *Energy Environ. Sci.* 4 (2011) 858–861.
- [29] D. Li, Y.N. Xia, *Nano Lett.* 4 (2004) 933–938.
- [30] Y.M. Chen, Z. Li, X.W. Lou, *Angew. Chem. Int. Ed.* 127 (2015) 10667–10670.
- [31] C.J. Niu, J.S. Meng, X.P. Wang, C.H. Han, M.Y. Yan, K.N. Zhao, X.M. Xu, W.H. Ren, Y.L. Zhao, L. Xu, Q.J. Zhang, D.Y. Zhao, L.Q. Mai, *Nat. Commun.* 6 (2015) 7402.
- [32] L.X. Yang, Y. Xiao, S.H. Liu, Y. Li, Q.Y. Cai, S.L. Luo, G.M. Zeng, *Appl. Catal. B: Environ.* 94 (2010) 142–149.
- [33] W.L. Yang, L. Zhang, Y. Hu, Y.J. Zhong, H.B. Wu, X.W. Lou, *Angew. Chem. Int. Ed.* 51 (2012) 11501–11504.
- [34] C.T. Gao, X.D. Li, B.G. Lu, L.L. Chen, Y.Q. Wang, F. Teng, J.T. Wang, Z.X. Zhang, X.J. Pan, E.Q. Xie, *Nanoscale* 4 (2012) 3475–3481.
- [35] X. Zeng, L.Q. Hunag, C.N. Wang, J.S. Wang, J.T. Li, X.T. Luo, *ACS Appl. Mater. Interfaces* 8 (2016) 20274–20282.
- [36] J.M. Deitzel, W. Kosik, S.H. McKnight, N.C.B. Tan, J.M. DeSimone, S. Crette, *Polymer* 43 (2002) 1025–1029.
- [37] J.H. Chen, X.N. Yu, X.C. Zhu, C.H. Zheng, X. Gao, K.F. Cen, *Appl. Catal. A: Gen.* 507 (2015) 99–108.
- [38] J.C. Fu, J.L. Zhang, Y. Peng, C.H. Zhao, Y.M. He, Z.X. Zhang, X.J. Pan, N.J. Mellorsb, E.Q. Xie, *Nanoscale* 5 (2013) 12551–12557.
- [39] P.P. Jing, J.L. Du, J.B. Wang, W. Lan, L.N. Pan, J.N. Li, J.W. Wei, D.R. Cao, X.L. Zhang, C.B. Zhao, Q.F. Liu, *Nanoscale* 7 (2015) 14738–14746.
- [40] Z.X. Wu, W.D. Wu, W.J. Liu, C. Selomulya, X.D. Chen, D.Y. Zhao, *Angew. Chem. Int. Ed.* 52 (2013) 13764–13768.
- [41] Z.F. Huang, J.J. Song, L. Pan, F.L. Lv, Q.F. Wang, J.J. Zou, X.W. Zhang, L. Wang, *Chem. Comm.* 50 (2014) 10959–10962.
- [42] Y.L. Cheng, J.T. Chen, X.B. Yan, Z.M. Zheng, Q.J. Xue, *RSC Adv.* 3 (2013) 20606–20612.